3D designature and deghosting in complex geology: application to Brazilian Equatorial margin data

Yamen Belhassen, Ihani Souza, Roberto Pereira, Erick Tomaz, Diego Carotti, Daniela Donno, Ibrahim Zoukaneri, CGG*

This paper was prepared for presentation during the 15th International Congress of the Brazilian Geophysical Society held in Rio de Janeiro, Brazil, 31 July to 3 August, 2017.

Abstract

Removing the source signature and source/receiver ghosts is crucial to determine accurate earth reflectivity from marine seismic acquisition. In complex geological areas, effective designature and deghosting should take into account the 3D nature of the seismic response. In this paper, we consider a marine dataset from the Brazilian Equatorial margin, where the seismic response is characterized by many diffractions associated with carbonate reefs below the rugose sea-floor with canyons. We propose a joint 3D directional source designature and deghosting followed by 3D receiver deghosting. From our results, we conclude that in such geologically complex areas, directional 3D designature is preferred to attenuate bubble energy effectively and homogeneously across all cables. Moreover, 3D source and receiver deghosting is vital to recover the full frequency bandwidth of the data and enhance sharp diffractions without introducing artifacts.

Introduction

Source designature as well as source and receiver deghosting are very important steps in broadband seismic data processing, aiming at retrieving the true earth response.

In complex geological areas such as the Brazilian Equatorial margin, a dense network of shallow canyons and shallow carbonate reefs generate several multi-directional diffractions. Effective designature and source/receiver deghosting of such a complex seismic response requires the use of methods that honor the 3D source directivity and the true 3D propagation of the data.

Conventional designature consists of applying a single 1D filter for all the streamers, thus considering a vertical take-off-angle approximation. This approximation fails to account for the source directivity and may lead to residual bubble energy on outer cables associated with large take-off angles (Lacombe et al. 2008).

Nowadays, deghosting the seismic data on both source and receiver sides is common practice in pre-processing. It allows us to fill the spectral notches created by the ghosts on both source and receiver sides, recovering a broader frequency bandwidth. Two-dimensional algorithms using a bootstrap approach are widely used (Wang et al. 2013). However, when strong 3D effects are present, deghosting algorithms that take into account 3D propagation are necessary to avoid introducing ringing artifacts.

In this work we show the improvement achieved on a dataset with complex geology from the Brazilian Equatorial margin (Barreirinhas basin - Figure 1), when using a joint 3D source designature and deghosting (Poole et al. 2015) followed by 3D receiver deghosting (Wang et al. 2014, Poole et al 2015).

Methodology

The conventional methodology for removing the source signature and the free-surface reflections includes 1D designature followed by 2D source and receiver deghosting. In this section we first introduce the limitations of conventional methods, and then present a new solution based on joint 3D designature and source deghosting (Poole et al. 2015) followed by 3D receiver deghosting (Wang et al. 2014).

The use of a 1D filter to remove the source signature from the recorded data, known as vertical designature, assumes a zero take-off-angle. This approximation generally gives reasonable results for near offset reflections and central cable data. However, due to the geometry of the array the source directivity is known to be anisotropic. This leads to wavelet distortion at wide take-off angles, for instance in the outer cable data and at far offsets. Here we refer to source designature as the process of removing the effect of the air-gun array response alone.

Conventional deghosting methods are based on 2D assumptions. The 2D approximations do not account for the 3D propagation of the wavefields and the directivity of the source. Therefore, in complex areas with strong 3D effects, 2D deghosting is less effective at properly removing the reflections from the sea's free-surface. Recent 2D deghosting algorithms (Wang et al. 2013) work in the Tau-Px domain, with Px being the wavefield slowness in the inline direction. The main reason for this choice is that, for a given local t-x window of data, large variations of emergent angles are better separated in the Tau-Px domain than in the t-x domain.

On the source side, Poole et al. (2015) proposed a joint 3D source designature and deghosting method. The algorithm works in the 3D Tau-Px-Py domain. As the 3D Tau-Px-Py transform might be impaired by coarse shotpoint coverage in the crossline direction, Poole et al. (2015) assume symmetry between the take-off angles at the source location and the emergent angles at the receiver location. In this way, the slowness at the source side can be computed as the opposite of the slowness at the receiver side: Px,s = - Px,r and Py,s = - Py,r. To measure the directivity effect of the source, the algorithm uses notional sources computed from the near field hydrophone data, following the approach of Ziolkowski et al. (1982). The reader might refer to Poole et al. (2013) for more details.

On the receiver side, the method proposed by Wang et al. (2014) for 3D receiver deghosting also works in the Tau-Px-Py domain, with Px and Py being the inline and crossline slowness components at the receiver side. Unlike the 2D deghosting method, the 3D method assumes Py values different from zero. The algorithm is based on a least-squares inversion scheme, similar to the one described by Poole et al. (2015). The coarse spatial sampling at the receiver side is overcome by applying a low-rank optimization scheme that reduces the model parameters. Then, the inversion is done sequentially from low frequencies to high frequencies, hence guiding the inversion towards the optimum solution.

Application to Brazilian Equatorial margin dataset

The Barreirinhas basin is located in the Southern part of the Brazilian Equatorial margin (Figure 1a). It is characterized by shallow carbonate reefs beneath the rugose water bottom associated with canyons. Such a complex geology generates multi-directional diffracted energy that is back-scattered to the surface, making the deghosting process challenging.

The seismic acquisition layout consisted of a variable-depth streamer with twelve 8 km long cables, and nominal streamer separation of 100 m. Flip-flop shots were fired every 50 m. The shot depth was 7 m, and the receiver depths ranged from 8 m to 50 m. The acquisition area covered around 14500 km^2 and the most geologically complex areas were found in the western and southern parts (Figure 1b).

We first consider the results after the application of designature only. In Figure 2, we compare the result after 3D designature (Figure 2c) with conventional 1D designature (Figure 2b). We display mid-channel data (4000 m offset) with their corresponding autocorrelations, in a complex canyon area (on the left part of each sub-figure) and in a flatter and deeper water-bottom area (on the right part). We can clearly see some remaining bubble energy in the result of the conventional method indicated by an arrow in Figure 2b.

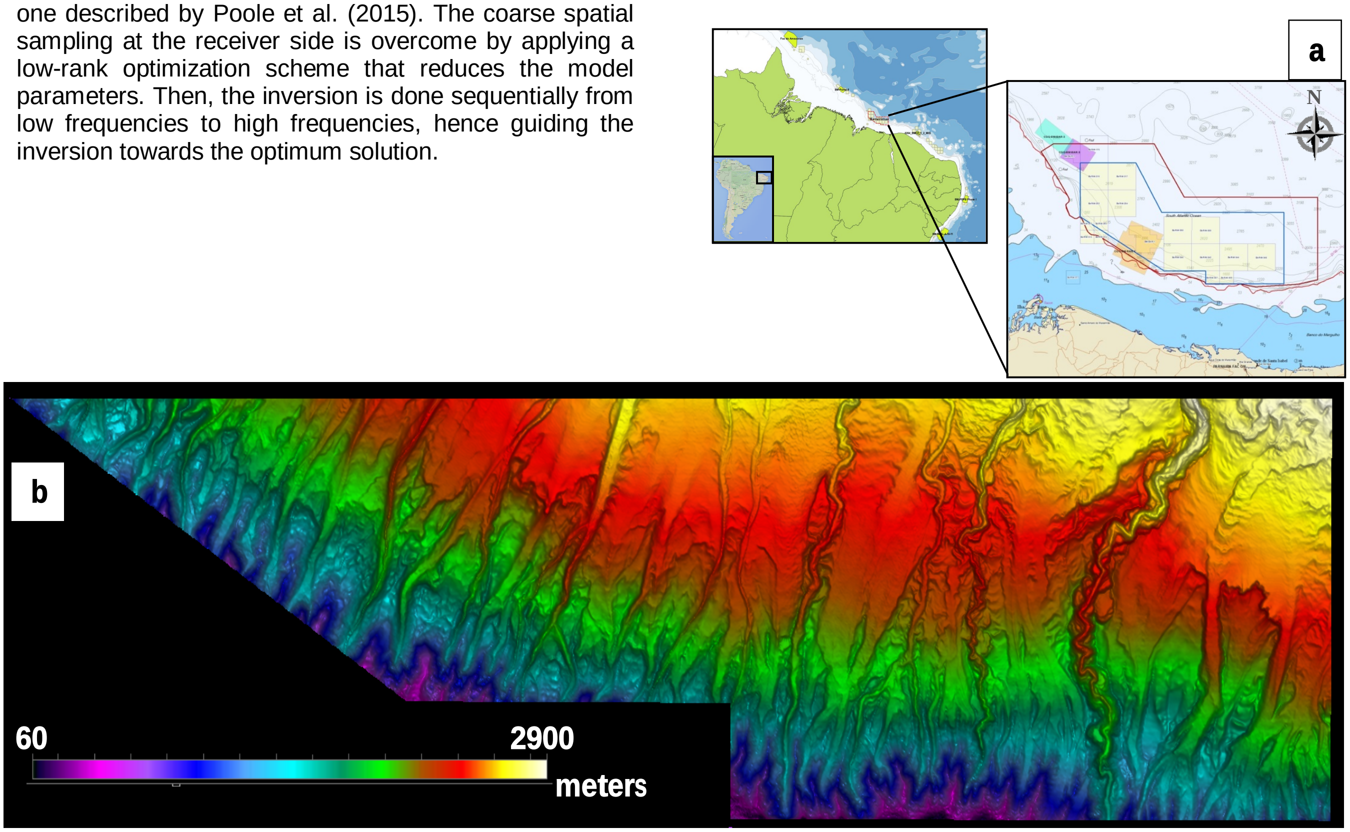

Figure 1: Application to Brazilian equatorial margin dataset (Barreirinhas basin): (a) survey and permit area and (b) rugose water bottom. (Courtesy of CGG MCNV)

More accurate removal of the bubble is observed in the result of the 3D approach, especially in the area with more complex geology. This improvement is mainly due to the fact that the directivity effect is neglected during the 1D signature estimation, but not in the 3D signature estimation.

Analyzing both central and outer cable data of a near channel (250 m offset), we can appreciate the effectiveness of 3D designature and source/receiver deghosting (Figure 3) compared to the 2D flow. Ringing appears after 2D deghosting particularly on the outer cable (Figures 3a, 3b) while a clearer result is obtained when using 3D deghosting, with sharper diffractions (Figures 3c and 3d).

The results after the 3D method are further analyzed in Figure 4, by looking at a stack and CMP gathers in an area with highly diffracted and out-of-plane energy. Both the 2D and 3D methods effectively attenuated the ghost energy; however the proposed 3D method better handled all of the diffractions corresponding to the complex carbonate reefs, without introducing ringing artifact. The diffraction tails were better deghosted with the 3D algorithm (Figure 4c) compared to the 2D method (Figure 4b), where some ringing can be observed.

Looking at the NMO-corrected CMP gathers, less ringing is visible near the water bottom reflection and sharper diffractions are obtained with the 3D method (Figure 4f) comparing to the 2D method (Figure 4e).

The benefit of 3D deghosting is further observed in the Kirchhoff stacked image. The pre-migration ringing near the diffraction tails generated by the 2D deghosting remains after migration (Figure 5a). Migration from the 3D deghosted data is free of artifacts (Figure 5b).

Conclusions

In this paper we have shown that designature and deghosting can be challenging in areas of complex geology and with strong 3D effects. For such scenarios, the use of processing algorithms that are able to account for the 3D nature of the data is essential in obtaining good quality results. Those observations were made based on our case study in the Brazilian Equatorial margin.

We have shown that 3D source designature is more effective at reducing bubble energy at far offsets and on outer cables than 1D designature, as it accounts for the 3D source directivity. Moreover, 3D source and receiver deghosting allow us to recover the full frequency bandwidth of the data without introducing artifacts.

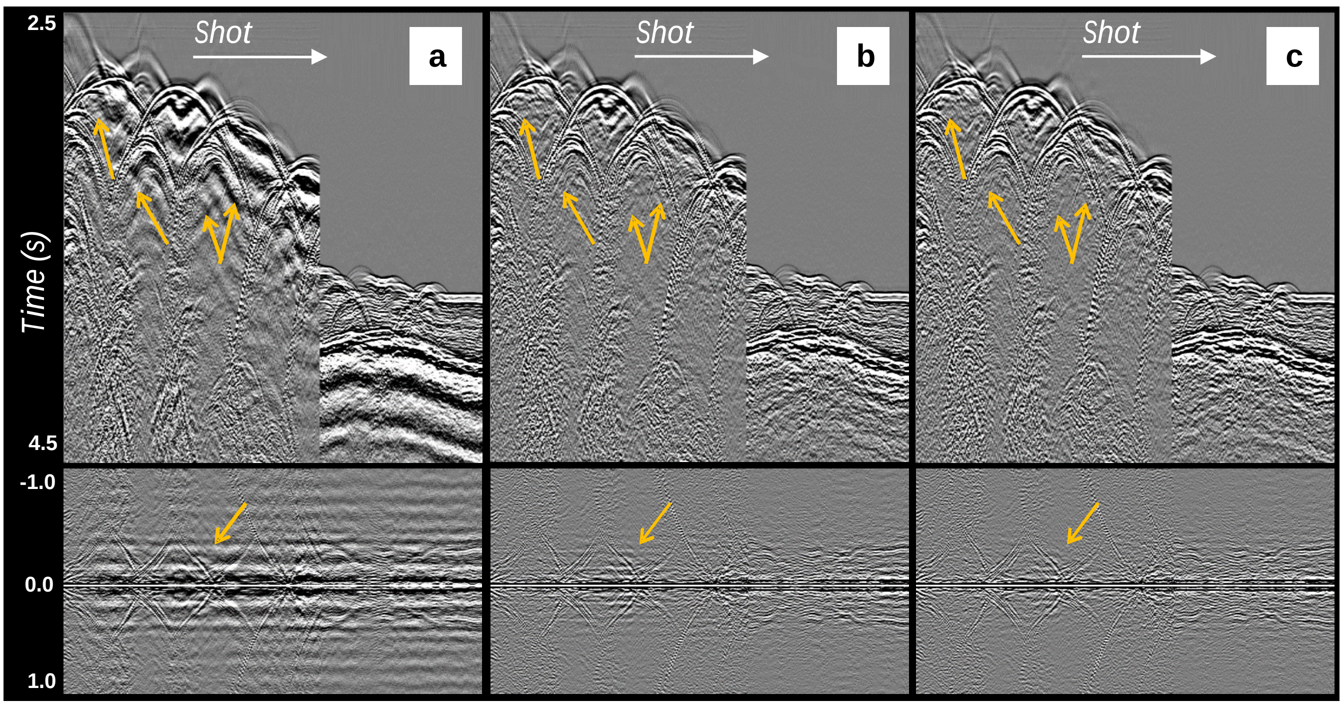

Figure 2: Mid-channel displays (4000 m offset) and their autocorrelation for (a) input data, (b) data after 1D designature, and (c) data after 3D designature. Arrows in the upper figures indicate areas of the data where the 3D designature gave the most effective results in removing the bubble. The remnant bubbling energy is also visible in the autocorrelation displays, when comparing 1D designature with 3D designature. The left part of each subfigure corresponds to a complex canyon area, while the right part corresponds to an area with a flatter and deeper water-bottom. (Courtesy of CGG MCNV)

Acknowledgments

We would like to thank CGG Data Library for permission to publish this work and James Cooper, Fabien Marpeau and Anderson Cavalcante for their support.

References

LACOMBE, C., HOEBER, H., CAMPBELL, S. & S. BUTT, 2008, Target oriented directive designature: 70th EAGE Conference & Exhibition, Expanded Abstract, H012.

POOLE, G., DAVISON, C., DEEDS, J., DAVIS, K. & G. HAMPSON, 2013, Shot-to-shot directional designature using near field hydrophone data: 83rd Annual International Meeting, SEG, Expanded Abstracts, 4236-4240.

POOLE, G., COOPER, J., KING, S. & P. WANG, 2015, 3D source designature using source-receiver symmetry in the shot tau-px-py domain: 77th EAGE Conference & Exhibition, Expanded Abstract, Th-N103-13.

WANG, P., RAY, S., PENG, C., LI, Y. & G. POOLE, 2013, Premigration deghosting for marine data using a bootstrap approach in tau-p domain: 83rd Annual International Meeting, SEG, Expanded Abstracts, 4221-4225.

WANG, P., RAY, S. & K. NIMSAILA, 2014, 3D joint deghosting and crossline interpolation for marine single-component streamer data: 84th Annual International Meeting, SEG, Expanded Abstracts, 3594-3598.

ZIOLKOWSKI, A., PARKES, G. E., HATTON, L. & T. HAUGHLAND, 1982, The signature of an air-gun array: computation from near-field measurements including interactions: Geophysics, 47, 1413-1421.

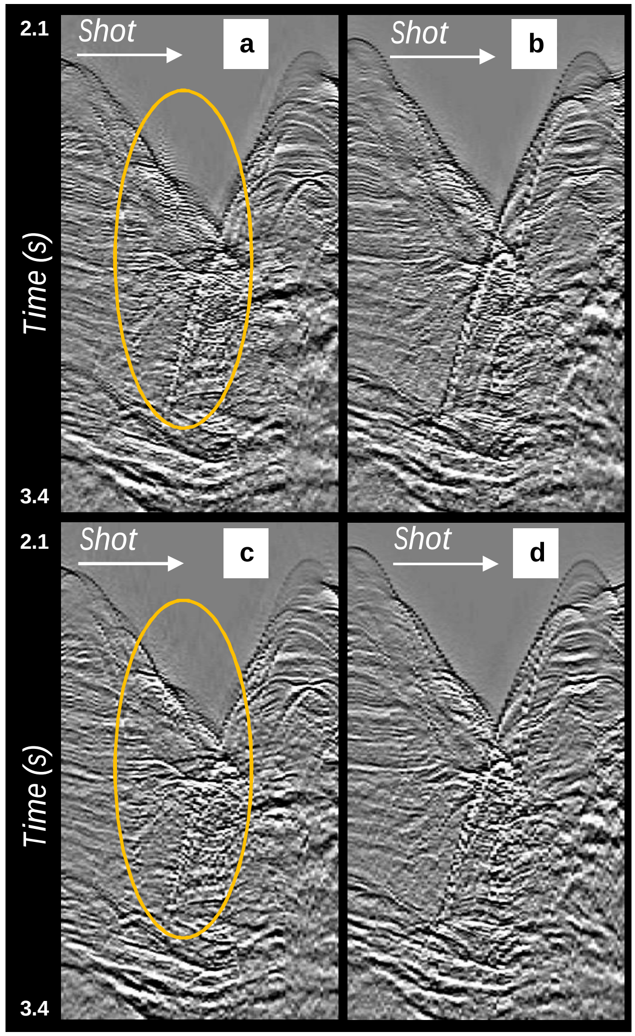

Figure 3: Comparison between 2D and 3D results on near-offset channels. Outputs of 1D designature and 2D source/receiver deghosting for (a) an outer cable and (b) a central cable. Outputs of 3D designature and source/receiver deghosting for (c) an outer cable and (d) a central cable. The yellow circle highlights areas on the outer-cable result where the 2D method introduces some ringing artifacts, due to presence of many 3D out-of-plane diffractions. (Courtesy of CGG MCNV)

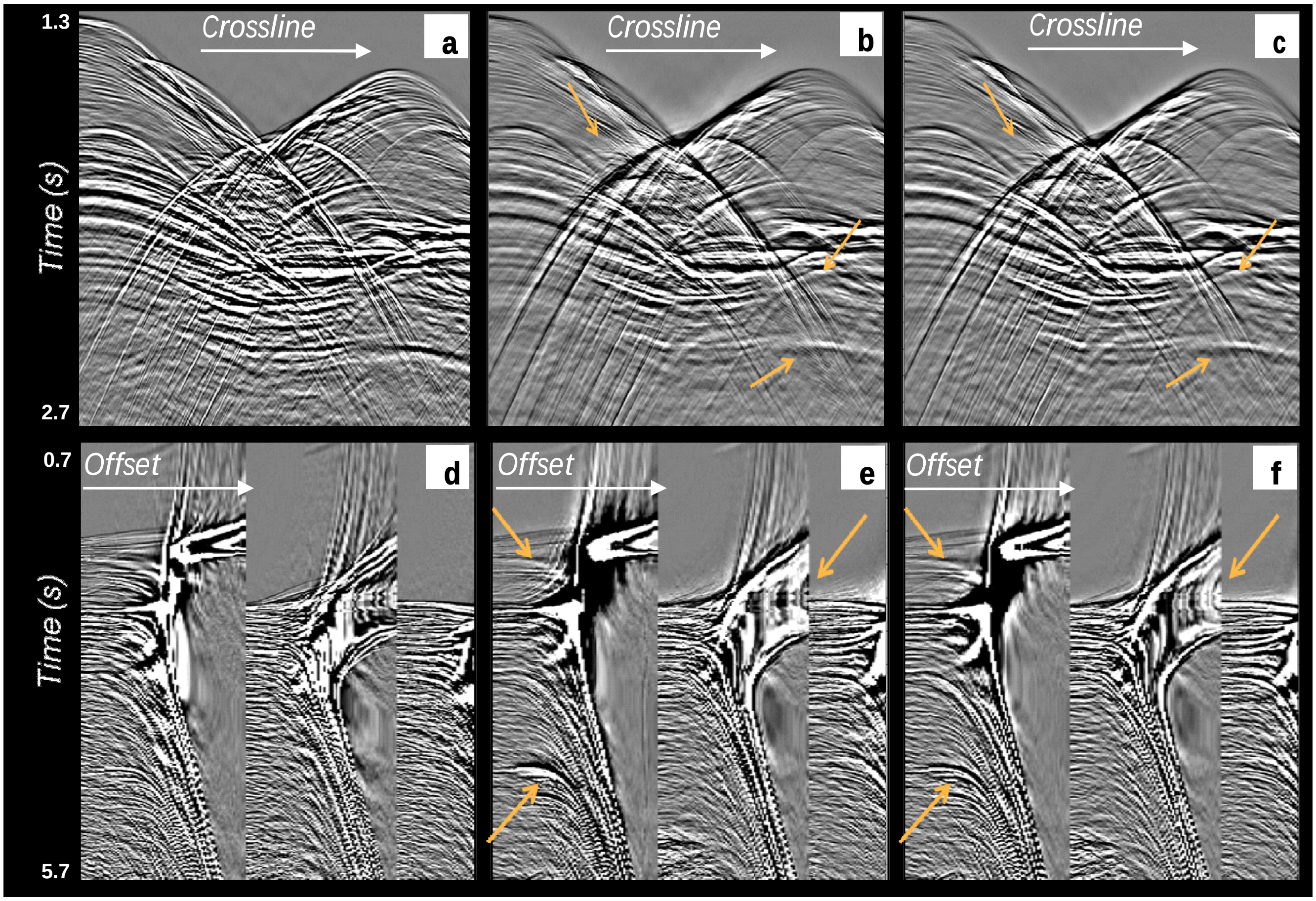

Figure 4: Comparison between 2D and 3D results. (a) Stack input data, (b) after 1D designature and 2D source/receiver deghosting, and (c) after 3D designature and source/receiver deghosting. NMO-corrected CMP gathers for (d) input data, (e) after 2D flow, and (f) after 3D flow. The yellow arrows highlight areas where the 2D method does not perform as expected and introduces some artifacts because of the strong 3D nature of reflections and diffractions in this area. (Courtesy of CGG MCNV)

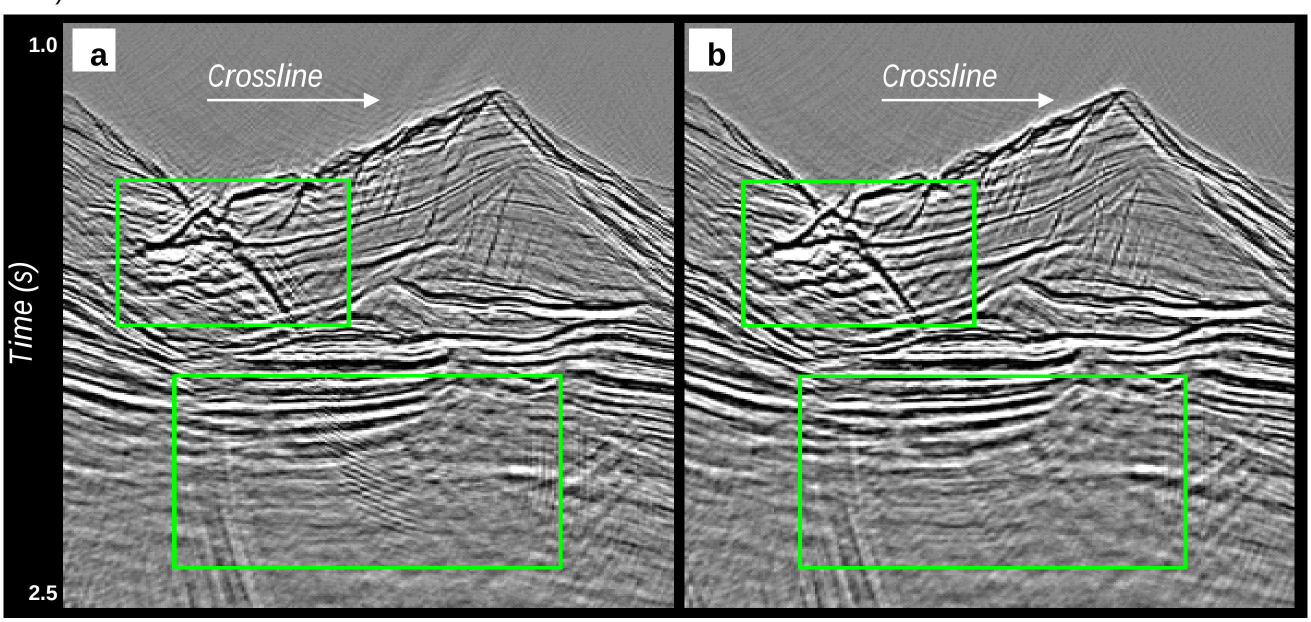

Figure 5: Stack from 2D Kirchhoff time migration (a) after 1D designature and 2D source and receiver deghosting, and (b) after joint 3D source designature and deghosting followed by 3D receiver deghosting. The effects of the improved results after the use of the 3D algorithms are especially visible in the highlighted areas of the image. (Courtesy of CGG MCNV)